UNIZIK JOURNAL OF ENGINEERING AND APPLIED SCIENCES (UJEAS)

Research Article

Inhibition of Mild Steel Corrosion in Alkaline Media Using Imidazolium-Based Ionic Liquid

Chizoba S. Okafor, Okechukwu D. Onukwuli, Loveth N. Emembolu, Chukwunonso O. Aniagor.

Special Issue

A Themed Issue in Honour of Professor Onukwuli Okechukwu Dominic (FAS).

This special issue is dedicated to Professor Onukwuli Okechukwu Dominic (FAS), marking his retirement and celebrating a remarkable career. His legacy of exemplary scholarship, mentorship, and commitment to advancing knowledge is commemorated in this collection of works.

Edited by
Chinonso Hubert Achebe PhD.
Christian Emeka Okafor PhD.

UJEAS

UNIZIK JOURNAL OF ENGINEERING
AND
APPLIED SCIENCES

UNIZIK Journal of Engineering and Applied Sciences 4(2), March (2025), 1802-1813
Journal homepage: https://journals.unizik.edu.ng/index.php/ujeas
PRINT ISSN: 2992-4383 || ONLINE ISSN: 2992-4391

Inhibition of Mild Steel Corrosion in Alkaline Media Using Imidazolium-Based Ionic Liquid

Chizoba S. Okafor[1,2], Okechukwu D. Onukwuli[2], Loveth N. Emembolu[2*], Chukwunonso O. Aniagor[2*]

[1]Federal Government College of Education (Technical), Isu, Ebonyi State, Nigeria

[2]Department of Chemical Engineering, Nnamdi Azikiwe University, P.M.B. 5025, Awka, Nigeria

***CorrespondingAuthor's E-mail:** co.aniagor@unizik.edu.ng; ln.emembolu@unizik.edu.ng

Abstract

This study investigated the inhibition potentials of synthesized ionic liquid on mild steel corrosion in 1 M NaOH media, and the inhibition efficiency was evaluated. The synthesized ionic liquid achieved a maximum inhibition efficiency of 93.4% at 0.7 g/L inhibitor concentration and 313 K. Potentiodynamic polarization and electrochemical impedance spectroscopy revealed significant improvements in corrosion resistance, with a maximum charge transfer resistance of 136.5 Ω·cm². Adsorption studies indicated that the inhibitor adhered to the Langmuir isotherm (R^2 = 0.9961), and this finding implies monolayer adsorption of inhibitor molecules onto a homogeneous metal surface. The activation energy increased with inhibitor concentration, from 6.81 kJ/mol at 0.1 g/L to 78.49 kJ/mol at 0.9 g/L. The exothermic adsorption process was characterized by a maximum adsorption energy of -90.71 kJ/mol at 0.7 g/L. Scanning electron microscopy revealed that the steel surface smoothened upon the addition of the inhibitor. Density Functional Theory analysis further confirmed the strong adsorption and reactivity of the inhibitor molecules.
Keywords: Corrosion inhibition, mild steel, ionic liquid, electrochemical analysis, alkaline media

1. Introduction

Mild steel corrosion during its application in construction, chemical processing, and pipeline systems is an issue of great concern (Shwetha et al., 2024). Due to the ease of metal dissolution/degradation in alkaline environments, the use of mild steel in such an environment poses significant challenges (Rihan & Nešić, 2006). Addressing this problem is vital to maintaining material durability, ensuring operational safety, and reducing maintenance costs. Traditional corrosion inhibitors, often based on synthetic chemicals, have been widely used to protect mild steel. However, concerns regarding their environmental impact and toxicity necessitate the exploration of more sustainable alternatives (Al-Amiery et al., 2024). Research on the application of ionic liquid solvents as alternative metal corrosion inhibitors is currently gaining attention (Kobzar & Fatyeyeva, 2021). Notably, ionic liquids offer several advantages over traditional inhibitors; hence, there is extensive application in various industrial applications. Their unique physicochemical properties, such as low volatility, high thermal stability, and tunable solubility, contribute to enhanced performance in extreme conditions where traditional inhibitors may degrade or evaporate (Gadioli et al., 2024). Additionally, ionic liquids can be designed with specific functional groups to improve their compatibility with different materials and environments (Roy & Ahmaruzzaman, 2022). Also, their strong ionic nature promotes the formation of stable, protective films on metal surfaces, and this development fosters superior corrosion resistance (Kobzar & Fatyeyeva, 2021). Furthermore, ionic liquids are often more environmentally friendly compared to conventional inhibitors, as they produce fewer toxic byproducts and can be recycled (de Jesus & Maciel Filho, 2022).

In the study by El-Nagar et al. (2024), the effectiveness and eco-friendly properties of imidazolium derivative ionic liquids with varying alkyl chain lengths were demonstrated while inhibiting the corrosion of carbon steel in acidic media. Zeng et al. (2021) and Azeez et al. (2018) evaluated the corrosion inhibition potentials of different imidazolium-based ionic liquids and were also tested on corroding mild steel in sulfuric acid media. Both studies noted that electrochemical experiments revealed an inhibition efficiency of 69.6 - 92.9 % at 303 K. However, despite the advancements, the potential of ionic liquids as inhibitors in highly alkaline environments, such as 1M

NaOH, has not been extensively studied. This represents a significant research gap, as alkaline environments are prevalent in many industrial processes, including cleaning operations, chemical synthesis, and wastewater treatment. Furthermore, the influence of specific ionic liquid structures on adsorption mechanisms and their correlation with corrosion inhibition efficiency in such media remains inadequately understood. To address these gaps, this study developed an ionic liquid that is based on methylamine, ethyl chloride, and imidazole. The study further explored the potential of the synthesized ionic liquid to inhibit mild steel corrosion in 1M NaOH media. The corrosion inhibition performance of the ionic liquid is assessed through thermometric, gravimetric, and electrochemical methods. Also, the adsorption isotherm and Density Functional Theory (DFT) calculations for the process were executed.

2. Materials and methods

2.1. Sample preparation

The mild steel sample (dimension: 4 cm × 3 cm × 0.1 cm), whose elemental distribution is presented in Table 1, was polished and degreased using emery paper and acetone, respectively.

Table 1: Elemental composition of the mild steel sample

S/N	Elemental composition	% elemental distribution
1.	Manganese (Mn)	0.13
2.	Phosphorus (P)	0.22
3.	Silicon (Si)	0.05
4.	Sulphur (S)	0.12
5.	Carbon (C)	0.24
6.	Chromium (Cr)	0.02
7.	Nickel (Ni)	0.07
8.	Iron (Fe)	99.15

2.2. Preparation of ionic liquid (IL) inhibitor

A mixture of 7 g methylamine, 10 g ethyl chloride, and 5 g imidazole was microwaved (power rating: 80%; and irradiation time: 7 min), and the product was mixed within dry ethyl acetate and centrifuged at 500 rpm and subsequently oven-dried at 70°C for 10 h. Afterwards, a 10 g/L stock solution of ionic liquid inhibitor was prepared, and test solutions for the corrosion studies were obtained via the serial dilution of the stock solution. The choice of the concentration range was informed by findings from preliminary investigations and literature reports.

2.3. Corrosion inhibition studies

This study was conducted via the thermometric and gravimetric (weight-loss) methods. The Thermometric measurements were conducted in line with the previously reported standard methodology (Emembolu et al., 2021; Kuhn & El Din, 1983), where the temperature of the solution was initially set to 30 ºC. Subsequently, both the reaction number (RN) and inhibitor efficiency (IE%) were respectively evaluated from Eq. (1) and (2). Similarly, the gravimetric corrosion inhibition study was conducted using the difference in the sample mass as an inhibition indicator. Afterwards, the weight loss, w (Eq. 3), corrosion rate, CR (Eq. 4), inhibition efficiency, %IE (Eq. 5) and surface coverage, θ (Eq. 6) were determined.

$$\mathrm{RN} = \frac{\mathrm{T_m} - \mathrm{T_i}}{\mathrm{t}} \qquad (1)$$

$$\mathrm{IE\%} = \left(1 - \frac{\mathrm{RN_{add}}}{\mathrm{RN_{free}}}\right) * 100 \qquad (2)$$

$$\mathrm{w} = \mathrm{w_i} - \mathrm{w_f} \qquad (3)$$

$$\mathrm{CR} = \frac{\mathrm{w_i} - \mathrm{w_f}}{\mathrm{At}} \qquad (4)$$

$$\mathrm{IE\%} = \frac{\mathrm{w_0} - \mathrm{w_1}}{\mathrm{w_0}} * 100 \qquad (5)$$

$$\theta = \frac{\mathrm{w_0} - \mathrm{w_1}}{\mathrm{w_0}} \qquad (6)$$

Where "T_m and T_i = final and initial temperatures (°C), respectively"; "t = time (min) to attain T_m"; "RN_{free} and RN_{add} = reaction numbers in the presence and absence of inhibitor, respectively"; "w_i and w_f = initial and final mass of corroding sample"; "w_1 and w_0 = weight loss values in the presence and absence of inhibitor, respectively"; "A = Surface area of corroding sample"; "θ = degree of surface coverage".

2.4. Instrumental characterization techniques

To further elucidate the surface morphology of the corroded mild steel in the absence and presence of the ionic liquid inhibitor, the samples were tested on a scanning electron microscope (model JEOL-JSM-5600, Germany). The synthesized ionic liquid was further identified using gas chromatography (JMS-T2000GC AccuTOF™ GC-Alpha, Germany) and UV spectrophotometer (Model VSI-501, USA).

2.5. Activation energy, heat of adsorption and adsorption isotherm

The activation energy is determined from the Arrhenius equation (Eq. 7), while Eq.(8) is useful for evaluating the heat of adsorption Q_{ads} ($kJmol^{-1}$). Similarly, the Langmuir, Frumkin and Flory-Huggins isotherm models presented in Eqs. (9 – 11), respectively, is applied to the obtained corrosion data.

$$\ln\left({CR_2}/{CR_1}\right) = \left({E_a}/{2.303R}\right)\left(\frac{1}{T_1} - \frac{1}{T_2}\right) \tag{7}$$

$$Q_{ads} = 2.303R\left[\log\left(\frac{\theta_2}{1-\theta_2}\right) - \log\left(\frac{\theta_1}{1-\theta_1}\right)\right] * \frac{T_2.T_1}{T_2-T_1} \tag{8}$$

$$\log\frac{C}{\theta} = \log C - \log K \tag{9}$$

$$\log\left((C) * \left(\frac{\theta}{1-\theta}\right)\right) = 2.303\log K + 2\alpha\theta \tag{10}$$

$$\log\left(\frac{\theta}{C}\right) = \log K + x\log(1-\theta) \tag{11}$$

Where "E_a = the activation energy"; "R = gas constant", "θ_1 and θ_2 = degrees of surface coverage"; "C = inhibitor concentration", and "k = adsorption equilibrium constant.

3. Result and Discussion

3.1. Investigation of process variable's effects on corrosion inhibition efficiency

Figure 1(a-c) respectively depicts the plots of the various process variables, vis-a-viz corrosion time, inhibitor concentration and temperature. Figure 1a shows an initial direct variation between the inhibition efficiency and corrosion time up to a maximum time of 3 h before gradually declining. The initial increase suggests the formation of a protective layer that inhibits corrosion on the steel surface within the first few hours. The subsequent decrease in efficiency could be due to the partial desorption of the inhibitor, degradation of the protective layer, or interference from the corrosive environment over extended exposure. Therefore, the optimum inhibition time of 3h was adopted throughout this study. In Figure 1b, a similar direct variable was observed between the inhibition efficiency and concentration up to an optimal concentration of 0.7 g/L before slightly declining. This result implies that at low inhibitor concentrations, the ionic liquid gradually adsorbs onto the steel surface, hence the reduced corrosion rate. However, beyond 0.7 g/L concentration, a marginal drop in the inhibition efficiency was observed. This slight decline in inhibition efficiency beyond the optimal concentration is due to the possible aggregation or reduced mobility of the ionic liquid molecules, thereby limiting their uniform distribution on the corroding sample. Hence, the optimal inhibitor concentration adopted in this study is 0.7 g/L. The relationship between the inhibition efficiency and temperature is inverse, with a significant drop as the temperature goes beyond 310 K, as shown in Figure 1c. This implies that at higher temperatures, the inhibitor readily desorbs from the surface of the corroding sample, thus making the protective layer less stable. Additionally, elevated temperatures accelerate the corrosive reactions and counteract the inhibition effect of the ionic liquid. This suggests the ionic liquid performs better at a lower temperature of 313K and might not be suitable for high-temperature applications without modifications.

3.2. Relationship between inhibitor concentration, E_a and Q_{ads}

Table 2 illustrates the relationship between inhibitor concentration, E_a, and Q_{ads} in the study. Notably, the E_a-value varies directly with the inhibitor concentration such that at 0.1 and 0.9 g/L, the E_a-value increased from 6814.57 to 78488.19 J/mol. The increase in E_a with concentration indicates that the corrosion process requires more energy to occur and that the ionic liquid forms a more effective protective barrier at higher concentrations, thus slowing down the corrosion reaction (Udunwa et al., 2024a). The Q_{ads}-values, as shown in Table 2, are negative across all concentrations, thus indicating exothermic adsorption. Meanwhile, the magnitude of Q_{ads} increases with concentration initially but decreases slightly at the highest concentration, 0.9 g/L. Specifically, at 0.1 g/L, the Q_{ads}-value is -38525.9 J/mol, and a peak value of -90711.2 J/mol was recorded at 0.7 g/L. However, at 0.9 g/L, the Q_{ads}-value decreases to -70128.3 J/mol. The negative Q_{ads} confirm that the binding of the inhibitor molecules onto the corroding metal surface is energetically favourable and spontaneous. The initial increase in the magnitude of Q_{ads} suggests stronger adsorption and more effective inhibitor-metal surface interaction as the concentration rises. Furthermore, the lower value recorded at 0.9 g/L is due to saturation effects or aggregation of the inhibitor molecules (Sanumi et al., 2021). It is thus concluded that by increasing the ionic liquid concentration, corrosion inhibition is improved by increasing the activation energy and enhancing adsorption strength (more negative Q_{ads}). However, optimal performance is observed at moderate concentrations of 0.7 g/L, beyond which the efficiency slightly diminishes.

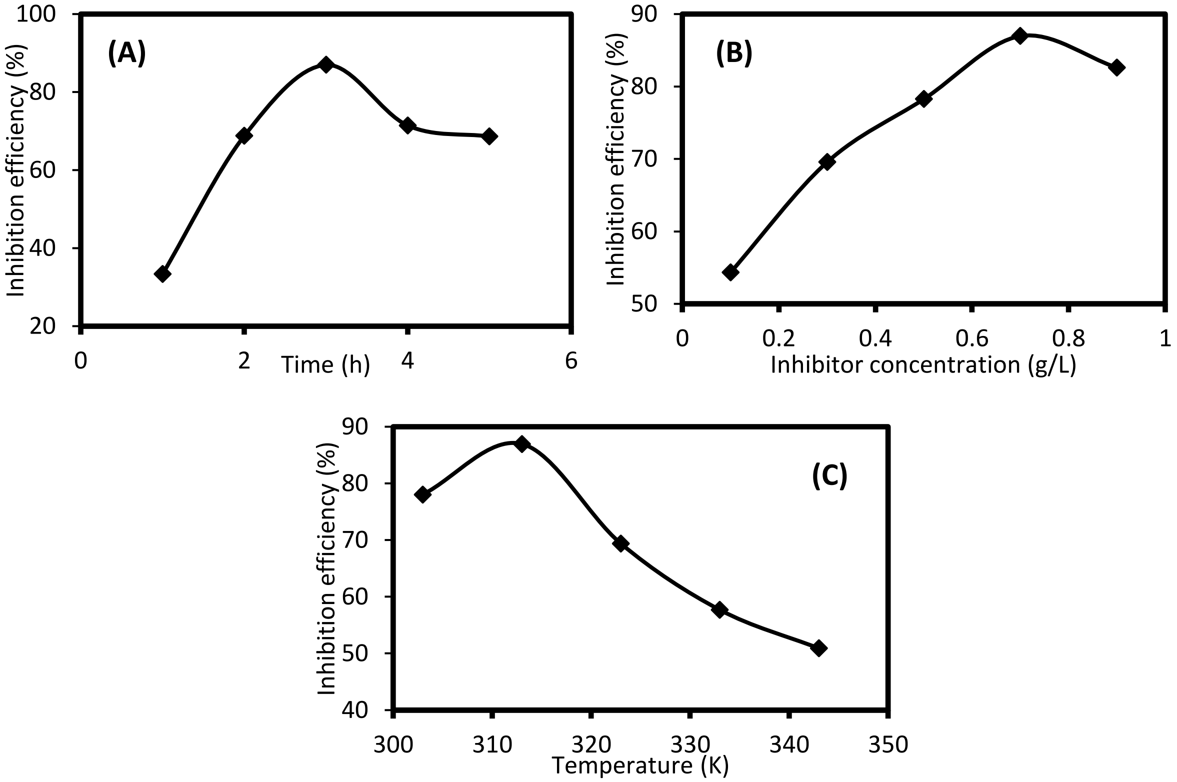

Figure 1: (A) Effect of time (B) inhibitor concentration and (C) temperature on corrosion inhibition efficiency

Table 2: The E_a and Q_{ads} -values recorded at varying inhibitor concentrations

Inhibitor concentration (g/L)	E_a (J/mol)	Q_{ads} (J/mol)
0.1	6814.57	-38525.9
0.3	31785.47	-52307
0.5	58077.47	-61964.2
0.7	121644.60	-90711.2
0.9	78488.19	-70128.3

3.3. Electrochemical measurement

3.3.1. Potentiodynamic polarization result

The black curve in Figure 2 (1 M NaOH, No inhibitor), which represents the metal's baseline behaviour in the blank, shows a relatively higher current density. This is typical of a higher corrosion rate. The red curve line in Figure 2 (0.3 g/L Inhibitor) shows a notable decrease in current density compared to the black curve. This observation indicates improved corrosion resistance, as the inhibitor seems to reduce the anodic or cathodic reaction rate. The blue curve Figure 2 (0.7 g/L Inhibitor) even showed a further reduction in current density compared to the red curve. This implies that an increased inhibitor concentration provides better protection by forming a stronger barrier to the corrosion process.

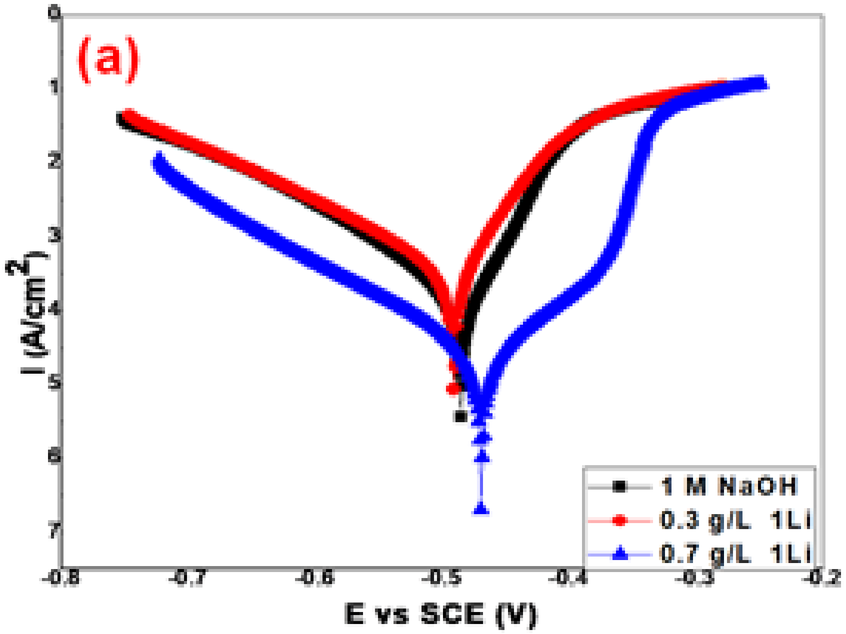

Figure 2: Potentiodynamic polarization plots

3.3.2. Electrochemical Impedance Spectroscopy (EIS)

Figure 3(a-c) and Table 3 show the respective electrochemical impedance spectra and parameters. The Nyquist plot (Figure 3a) displays the impedance (Z) spectra, both for the imaginary (Z_{im}) and the real part (Z_{re}). Accordingly, the charge transfer resistance is often deduced from the diameter of the semicircular plots (Feliu Jr, 2020). Notably, in the absence of an inhibitor, the semicircle is smaller, indicating lower impedance and less corrosion resistance. However, the semicircle diameter increases as the inhibitor concentration and the largest semicircle was recorded for 0.7 g/L inhibitor concentration (denoted by the blue line in Figure 3a). Emembolu et al. (2021) noted that high impedance and improved corrosion resistance are synonymous with larger semicircular spectra.

The modulus plot shows the magnitude of the impedance (|Z|) versus frequency (Hz) and highlights the overall impedance behaviour over a range of frequencies (Abbas et al., 2024). Figure 3b shows that the impedance magnitude is lower across all frequencies in the blank solution. However, with the introduction of the inhibitor, the impedance magnitude significantly improved. This improvement was progressively significant at higher concentrations of the inhibitor, thus indicating better protection against corrosion. Notably, Sajadi et al. (2022) made a similar observation during the study of corrosion inhibition in mild steel in an acidic medium using plant extracts. The phase angle plot (Figure 3c) shows the phase angle of the impedance versus frequency (Hz). In the absence of an inhibitor, the phase angle peaks at intermediate frequencies and indicates a blend of capacitive and resistive behaviour. However, with the introduction of varying concentrations of ionic liquid inhibitors, the peak phase angle increased at intermediate frequencies. Meanwhile, the increase in the peak phase angle was higher with increasing inhibitor concentrations, thus indicating improved capacitive behaviour and better corrosion protection. Wang et al.

(2020) and Al Otaibi and Hammud (2021) both reported significant variations in phase angle with inhibitor concentration. It is thus concluded that the developed ionic liquid efficiently inhibited mild steel corrosion alkaline media. Higher concentrations of the inhibitor result in increased impedance and better corrosion protection, as evidenced by the larger semicircles in the Nyquist plot, higher impedance magnitudes in the Modulus plot, and higher peak phase angles in the Phase angle plot.

Table 3: Electrochemical parameter for the corrosion process

System	R_s (Ω cm^2)	R_{ct} (Ω cm^2)	N	IE (%)	E_{corr} (mV)	I_{corr} (μA/cm$_2$)	IE%
1 M NaOH	1.659	41.2	0.89		- 445.2	185.4	
0.3 g/L IL	1.875	78.7	0.88	47.6	- 464.3	82.6	55.4
0.7 g/L IL	2.644	136.5	0.89	69.8	- 486,5	45.6	75.4

NB: IL is an abbreviation for Ionic Liquid

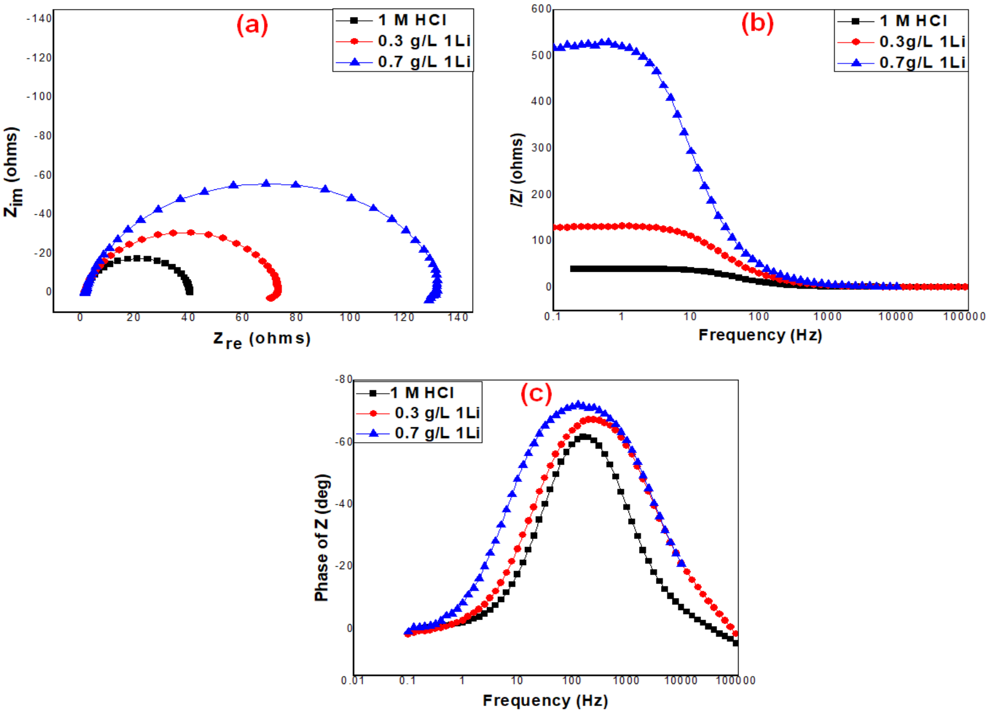

Figure 3: The Electrochemical impedance spectra for (a) Nyquist, (b) Modulus and (c) Phase angle plots

3.4. Sample characterization result

3.4.1. Scanning electron micrograph (SEM) analyses

Figure 4(a) shows that the mild steel surface appears rough and uneven. The image was also marked by numerous dark spots and pits. These characteristics indicate substantial corrosion damage. For instance, the presence of pits suggests localized corrosion as they represent areas where the metal has been significantly dissolved with an attendant weakening of the metal. Notably, the overall structure of Figure 4(a) is severely deteriorated due to the uncontrolled breakdown of the protective oxide layer. In Figure 4b, the mild steel surface appears significantly smoother and more uniform compared to the blank. This smoother surface indicates reduced corrosion due to the presence of an inhibitor. Additionally, the visible reduction in dark spots and pits suggests that the ionic liquid inhibitor has effectively mitigated pitting corrosion. The uniform appearance further implies enhanced corrosion resistance.

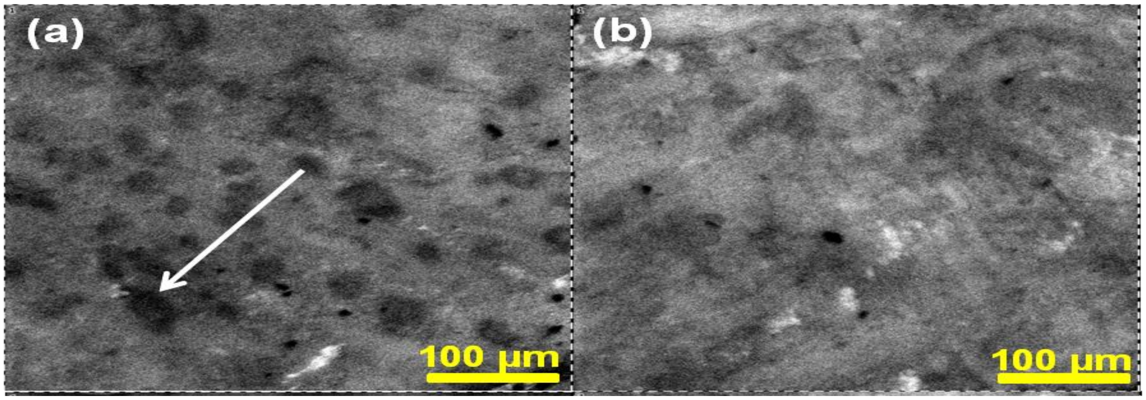

Figure 4: SEM image of corroded metal in the (a) absence and (b) presence of inhibitor

3.4.2. UV and gas chromatographic (GC-MS) analyses of the ionic liquid

The UV (Figure 5a) and GC-MS (Figure 5b) spectra of the ionic liquid, together with the GC-MS data presented in Table 4, reveal significant insights into their electronic structures and potential effectiveness as inhibitors. The observed adsorption maxima at 206 nm in Figure 5a and the peak point in Figure 5b both indicate the presence of 9-Octadecenoic acid methyl ester. This absorption maxima further suggests the existence of π-π* transitions associated with aromatic or conjugated systems. The UV absorbance patterns also reflect the stability of the ionic liquids in solution since the absorption maxima are recorded at lower wavelengths (206 nm). This attribute explains the successful application of the ionic liquid in corrosive environments (Araujo et al., 2022).

Table 4: The GC-MS data for 9-Octadecenoic acid methyl ester

Retention time (min)	% composition	CAS	Molecular weight (g/mol)	Molecular formula
15.1279	43.9756	002462-84-2	296.49	$C_{19}H_{36}O_2$

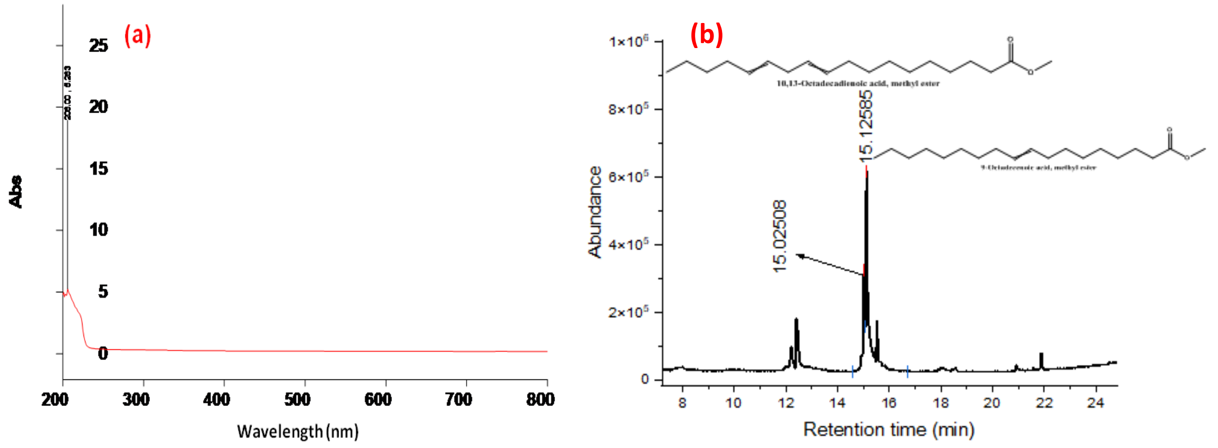

Figure 5: The presence of 9-Octadecenoic acid methyl ester depicted in the (a) UV and (b) GC-MS spectra

3.5. Density Functional Theory (DFT) parameters and corrosion control study

The electronic properties and reactivity of the inhibitor are deduced from the data presented in Table 5 and Figure 5. According to Emembolu et al. (2020), better reactivity and corrosion inhibition are synonymous with a smaller energy gap (ΔE). (Araujo et al., 2022). Considering the visual representations, Figure 5(a) shows the neutral and protonated molecular structures of the ionic liquid inhibitor. Accordingly, the interaction of the inhibitor with the metal surface is a function of the inhibitor's molecular orientation (Ravi et al., 2023). The electron density distribution within the molecule, as shown in Figure 5(b), presents high electron density regions (blue areas) where the molecule is most reactive. Furthermore, the regions highlighted in blue and yellow in Figure 5(c) are HOMO regions where electron donation is likely to occur during chemical interactions. Similarly, the highlighted portion of Figure 5(d) depicts the areas of LUMO that are likely to accept electrons. The combined visualization of the HOMO and LUMO profiles (Figure 5e) highlights the regions where electron transfer is likely to occur. For the molecule adsorbed on a surface, the energy levels are determined as HOMO = -6.174 eV and LUMO = -0.711 eV, showing slight shifts attributed to interactions with the surface.

Table 5: Summary of DFT chemical quantum parameters

S/N	DFT parameter	Values obtained
1.	[a]HOMO (eV)	- 6.088
2.	[b]LUMO (eV)	- 0.763
3.	[c]ΔE (Energy gap) (eV)	5.325
4.	χ (Electronegativity) (eV)	3.426
5.	η (Hardness) (eV)	2.663
6.	$Ó_s$ (Softness) (eV)	0.376
7.	ώ (Electrophilicity) (eV)	0.856
8.	ΔN (Change in Electron Density) (eV)	0.671
9.	Ads.Energy (KJ/mol)	243.4

[a]Highest Occupied Molecular Orbital
[b]Lowest Occupied Molecular Orbital
[c]Energy gap

3.6. Impact of ionic liquid structure on inhibition efficiency

The structure of ionic liquids plays a crucial role in determining their inhibition efficiency. The nature of the cation, anion, and alkyl chain length significantly influences the adsorption behaviour of ILs on the metal surface, thereby affecting their corrosion inhibition performance. ILs with longer alkyl chains tend to form more stable and compact protective films due to enhanced hydrophobic interactions, leading to improved corrosion resistance. The presence of functional groups such as imidazolium rings facilitates strong electrostatic interactions and hydrogen bonding with the metal surface. Furthermore, the electron density distribution and the HOMO – LUMO energy gap influences the reactivity and interaction strength between the inhibitor molecules and the metal sample. The Density Functional Theory (DFT) analysis in this study confirmed that the high inhibition efficiency exhibited by the synthesized ionic liquid is due to its higher electron density regions and lower energy gaps.

3.7. Adsorption isotherm

The adsorption isotherm modelling parameters and the associated model plots are presented in Table 6 and Figure 6, respectively. The performance of the respective models is measured based on the coefficient of determination (R^2) value. The Langmuir model, having R^2 value = 0.9961, indicates a very strong fit. Based on the aforementioned result, it is assumed that the binding of the inhibitor molecules occurs via monolayer adsorption with uniform sites and no interaction between adsorbed molecules (Langmuir, 1916). Similarly, the Frumkin model shows a slightly lower R^2 value compared to the Langmuir model and the α parameter, which accounts for lateral interactions between adsorbed molecules, suggests that such interactions may not dominate the adsorption mechanism since the value is quite minimal (α = 2.443). The Flory-Huggins model exhibits the lowest R^2 value (0.8583), indicating a comparatively weaker fit. This suggests that the adsorption process does not strongly align with the assumptions of this model (spatial distribution of adsorbed molecules).

In conclusion, the results emphasize that the adsorption process is likely dominated by uniform adsorption onto a homogeneous surface rather than influenced by molecular size or strong lateral interactions. This inhibition efficiency demonstrated in this study is comparable to those reported in the literature, as compiled in Table 7.

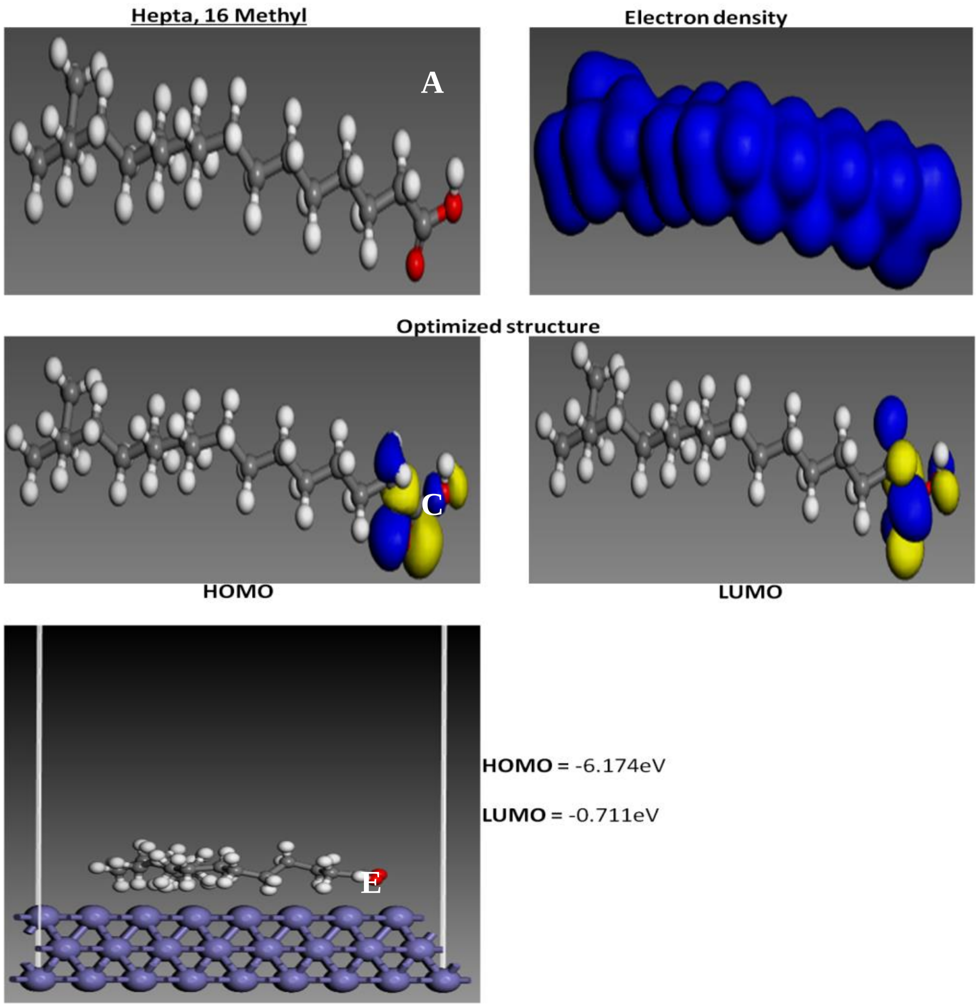

Figure 5: Electronic properties of the neutral and protonated form of ionic liquid inhibitor molecules (A), electron density (B), optimized HOMO structure (C) and optimized LUMO structure (D) and combined HOMO and LUMO profiles (E).

Table 6: Adsorption model parameters at 313 K

Langmuir	Frumkin	Flory-Huggins
R^2 = 0.9961	R^2 = 0.9886	R^2 = 0.8583
k = 0.9558	k = 0.216	k = 2.839
	α = 2.443	x = 1.2347

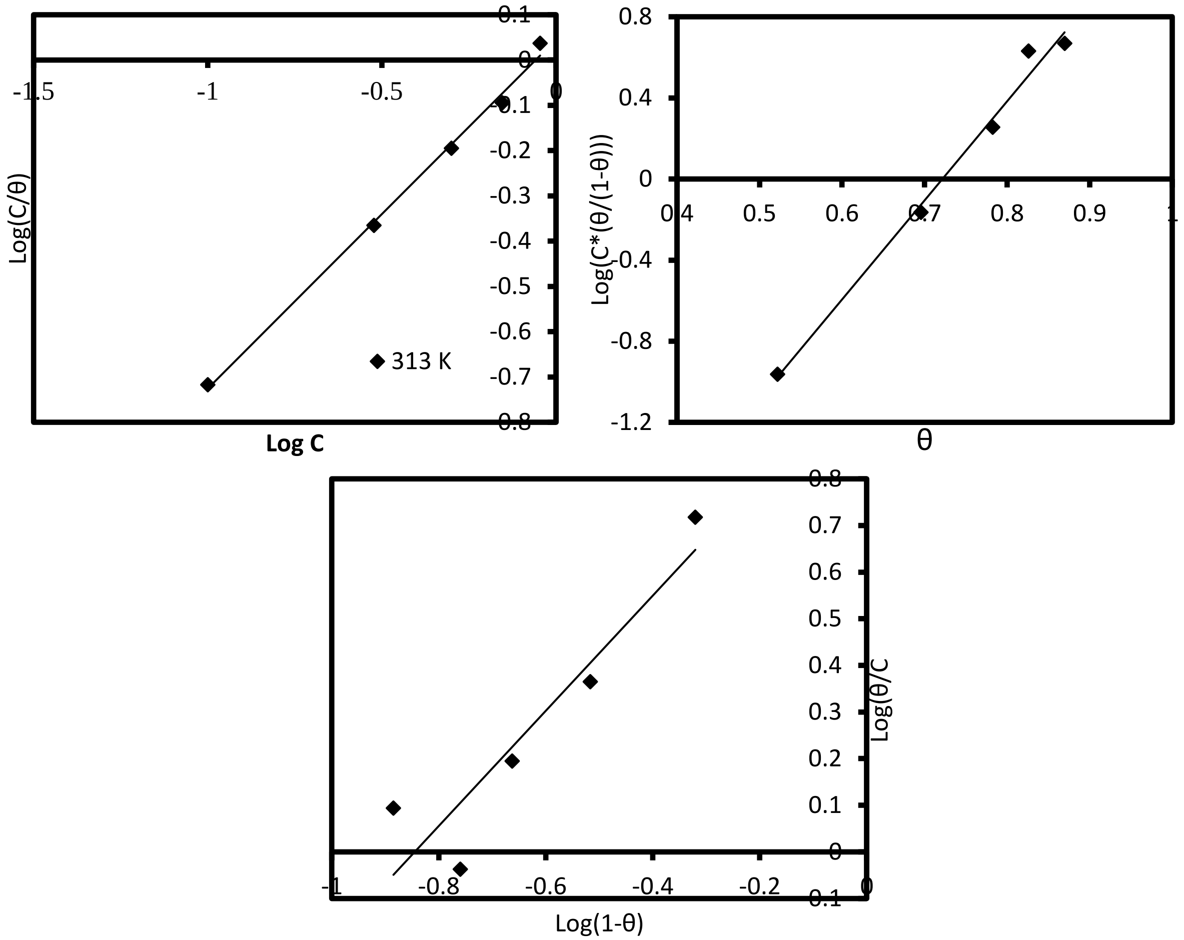

Figure 6: The adsorption isotherm plots for (A) Langmuir (B) Frumkin (C) Flory-Huggins model

Table 7: Comparison of the inhibition efficiency of ionic liquids reported in the literature

Ionic liquid	Corroding surface	Inhibitor conc (g/L)	Corrosion media	Inhibition efficiency (%)			References
				Gravimetric	[a]PDP	[b]EIS	
1-butyl-3-methylimidazolium tetrachloroindate	Aluminium alloy	0.8	Alkaline	88.46	82	82.35	(Udunwa et al., 2024b)
1-butyl-3-methylimidazolium p-toluenesulfonate	API 5L X70 steel	0.8	Acidic	80.36	84	85.93	(Udunwa et al., 2025)
1-butyl-3-methylimidazolium chloride	Aluminium alloy	0.8	Acidic	84.21	90	87.10	(Udunwa et al., 2022)
1-butyl-3-methylimidazolium tetrafluoroborate	Carbon steel	0.7	Alkaline	89.0	-	86.1	(Guo et al., 2017)
Methylamine imidazolium ethyl chloride	Mild steel	0.7	Alkaline	-	-	75.4	Present study

[a]Potentiodynamic polarization
[b]Electrochemical impedance spectroscopy

4. Conclusion

The findings suggest that ionic liquid inhibitors can be effectively utilized in industrial applications such as pipelines, chemical reactors, and marine environments where mild steel is exposed to alkaline conditions. Their high efficiency at low concentrations, environmental friendliness, and recyclability make them suitable for sustainable corrosion protection strategies. Despite the results obtained in this study, future studies should focus on testing other ionic liquid structures with varied cation-anion combinations to explore their corrosion inhibition efficiencies across different environments. The long-term stability and durability of these inhibitors under fluctuating temperature and pressure conditions should be investigated. Additionally, exploring the synergistic effects of ILs with other green inhibitors could lead to the development of more robust corrosion protection systems.

Acknowledgement

The authors acknowledge the use of OpenAI's ChatGPT for assistance in revising and improving the clarity and language of this manuscript. All intellectual content and final interpretations are solely the responsibility of the authors.

References

Abbas, Y., van Smeden, L., Verschueren, A. R., Zevenbergen, M. A., & Oudenhoven, J. F. (2024). Modeling Electrochemical Impedance Spectroscopy Using Time-Dependent Finite Element Method. *Sensors*, *24*(22), 7264.

Al-Amiery, A., Isahak, W. N. R. W., & Al-Azzawi, W. K. (2024). Sustainable corrosion Inhibitors: A key step towards environmentally responsible corrosion control. *Ain Shams Engineering Journal*, 102672.

Al Otaibi, N., & Hammud, H. H. (2021). Corrosion inhibition using harmal leaf extract as an eco-friendly corrosion inhibitor. *Molecules, 26*(22), 7024.

Araujo, R. B., Rodrigues, G. L., Dos Santos, E. C., & Pettersson, L. G. (2022). Adsorption energies on transition metal surfaces: towards an accurate and balanced description. *Nature Communications, 13*(1), 6853.

Azeez, F. A., Al-Rashed, O. A., & Nazeer, A. A. (2018). Controlling of mild-steel corrosion in acidic solution using environmentally friendly ionic liquid inhibitors: Effect of alkyl chain. *Journal of Molecular Liquids, 265*, 654-663.

de Jesus, S. S., & Maciel Filho, R. (2022). Are ionic liquids eco-friendly? *Renewable and Sustainable Energy Reviews, 157*, 112039.

El-Nagar, R. A., Khalil, N., Atef, Y., Nessim, M. I., & Ghanem, A. (2024). Evaluation of ionic liquids based imidazolium salts as an environmentally friendly corrosion inhibitors for carbon steel in HCl solutions. *Scientific reports, 14*(1), 1889.

Emembolu, L., Onukwuli, O., Umembamalu, C., & Aniagor, C. (2020). Evaluation of the corrosion inhibitory effect of Napoleonaea Imperalis leaf extract on mild steel in a 1.3 MH 2 SO 4 medium. *Journal of Bio-and Tribo-Corrosion*, *6*(4), 1-15.

Emembolu, L. N., Aniagor, C. O., Umembamalu, J. C., & Onyenanu, C. N. (2021). Electrochemical and statistical study of the inhibition effect of T. conophorum leaf extract on aluminum corrosion in acidic medium. *Safety in Extreme Environments*, 1-10.

Feliu Jr, S. (2020). Electrochemical impedance spectroscopy for the measurement of the corrosion rate of magnesium alloys: Brief review and challenges. *Metals*, *10*(6), 775.

Gadioli, A. O., de Souza, L. M., Pereira, E. C., Monteiro, S. N., & Azevedo, A. R. (2024). Imidazolium-based ionic liquids as corrosion inhibitors for stainless steel in different corrosive media: An overview. *Journal of Materials Research and Technology*.

Guo, Y., Xu, B., Liu, Y., Yang, W., Yin, X., Chen, Y., Le, J., & Chen, Z. (2017). Corrosion inhibition properties of two imidazolium ionic liquids with hydrophilic tetrafluoroborate and hydrophobic hexafluorophosphate anions in acid medium. *Journal of Industrial and Engineering Chemistry, 56*, 234-247.

Kobzar, Y. L., & Fatyeyeva, K. (2021). Ionic liquids as green and sustainable steel corrosion inhibitors: Recent developments. *Chemical Engineering Journal, 425*, 131480.

Kuhn, A., & El Din, A. S. (1983). Thermometric and calorimetric methods in electrochemical and corrosion studies. *Surface Technology, 20*(1), 55-69.

Langmuir, I. (1916). The constitution and fundamental properties of solids and liquids. Part I. Solids. *Journal of the American chemical society, 38*(11), 2221-2295.

Ravi, S., Peters, S., Varathan, E., & Ravi, M. (2023). Molecular interaction and corrosion inhibition of benzophenone and its derivative on mild steel in 1 N HCl: electrochemical, DFT and MD simulation studies. *Colloids and Surfaces A: Physicochemical and Engineering Aspects, 661*, 130919.

Rihan, R. O., & Nešić, S. (2006). Erosion–corrosion of mild steel in hot caustic. Part I: NaOH solution. *Corrosion Science, 48*(9), 2633-2659.

Roy, S., & Ahmaruzzaman, M. (2022). Ionic liquid based composites: A versatile materials for remediation of aqueous environmental contaminants. *Journal of environmental management*, *315*, 115089.

Sajadi, G. S., Naghizade, R., Zeidabadinejad, L., Golshani, Z., Amiri, M., & Hosseini, S. M. A. (2022). Experimental and theoretical investigation of mild steel corrosion control in acidic solution by Ranunculus arvensis and Glycine max extracts as novel green inhibitors. *Heliyon, 8*(10).

Sanumi, O. J., Saliu, O. D., & Makhatha, M. E. (2021). Alternative surface localization studies and electrochemical investigation of tyrosine hybridized poly (ethylene glycol) for corrosion inhibition of mild steel. *Journal of Materials Research and Technology*, *13*, 700-715.

Shwetha, K., Praveen, B., & Devendra, B. K. (2024). A review on corrosion inhibitors: types, mechanisms, electrochemical analysis, corrosion rate and efficiency of corrosion inhibitors on mild steel in an acidic environment. *Results in Surfaces and Interfaces*, 100258.

Udunwa, D. I., Onukwuli, O. D., & Anadebe, V. C. (2022). Synthesis and evaluation of 1-butyl-3-methylimidazolium chloride based ionic liquid for acid corrosion inhibition of aluminum alloy: Empirical, DFT/MD-simulation and RSM modeling. *Journal of Molecular Liquids, 364*, 120019.

Udunwa, D. I., Onukwuli, O. D., Menkiti, M. C., Nwanonenyi, S. C., Ezekannagha, C. B., & Aniagor, C. O. (2024a). Experimental, computational, and theoretical studies on the corrosion inhibition potential of green Gongronema latifolium extract as corrosion inhibitor for aluminum alloy in HCl solutions. *Journal of Molecular Structure*, *1302*, 137508.

Udunwa, D. I., Onukwuli, O. D., Nwanonenyi, S. C., & Ezekannagha, C. B. (2024b). Novel imidazole based ionic liquid as anti-corrosion additive for aluminum alloy: Combined experimental, DFT/MD simulation and soft computing approach. *Applied Surface Science Advances, 19*, 100578.

Udunwa, D. I., Onukwuli, O. D., Nwanonenyi, S. C., Ude, C. N., Arukalam, I. O., & Uche, R. (2025). Newly synthesized 1-butyl-3-methylimidazolium p-toluenesulfonate ionic liquid for acid corrosion of API 5L X70 steel: Experimental, DFT/MD-simulation, statistical and machine learning predictions. *Results in Surfaces and Interfaces, 18*, 100398.

Wang, X., Huang, A., Lin, D., Talha, M., Liu, H., & Lin, Y. (2020). Imidazolium-based ionic liquid as efficient corrosion inhibitor for AA 6061 alloy in HCl solution. *Materials, 13*(20), 4672.

Zeng, X., Zheng, X., Guo, L., Xu, Q., Huang, H., & Tan, B. (2021). Three imidazole ionic liquids as green and eco-friendly corrosion inhibitors for mild steel in sulfuric acid medium. *Journal of Molecular Liquids, 324*, 115063.